References and Notes

1. Smithsonian Institution, *SEAN (Sci. Event Alert Network) Bull.* **7**, 3 (1982).
2. D. F. Heath, A. J. Krueger, H. A. Roeder, B. D. Henderson, *Opt. Eng.* **14**, 323 (1975); A. J. Fleig, K. F. Klenk, P. K. Bhartia, D. Gordon, *NASA Ref. Publ. RP 1096* (1982).
3. Possible cloud constituents were considered to be SO_2, CS_2, COS, H_2S, H_2SO_4, HCl, HF, HBr, H_2, CO, and CO_2. All except SO_2 and CS_2 are transparent at TOMS wavelengths [H. Okabe, *Photochemistry of Small Molecules* (Wiley, New York, 1978)]. The SO_2 cross sections were obtained by C. Y. R. Wu and D. L. Judge [*Geophys. Res. Lett.* **8**, 769 (1981); unpublished data]. These cross sections are in agreement with measurements by M. M. Millan and R. M. Hoff (Atmospheric Environment Service, Downsview, Ontario) at 312.5 nm, but are 25 percent higher at 317.5 nm. Cross-section data on CS_2 were obtained from P. H. Wine, W. L. Chameides, and A. R. Ravishankara [*Geophys. Res. Lett.* **8**, 543 (1981); unpublished data].
4. K. L. Coulson, T. E. Defoor, J. Deluisi, *Eos* **63**, 897 (Abstr.) (1982).
5. I thank the Landsat/Nimbus Project Office and the General Electric, Bendix, and Systems and Applied Sciences Companies for their assistance in providing real-time processing of TOMS data. J. A. Gatlin provided the color TOMS images. Funding for real-time processing of North American TOMS orbits was provided by the NASA Office of Aerospace Technology.

17 September 1982; revised 13 December 1982

Venus: Global Surface Radio Emissivity

Abstract. *Observations of thermal radio emission from the surface of Venus, made by the Pioneer Venus radar mapper at a wavelength of 17 centimeters, show variations that are dominated by changes in surface emissivity. The regions of lowest emissivity (0.54 ± 0.05 for the highland areas of Aphrodite Terra and Theia Mons) correspond closely to regions of high radar reflectivity reported earlier. These results support the inference of inclusions of material with high electrical conductivity in the surface rock of these areas.*

As part of its normal operating sequence, the Pioneer Venus radar mapper experiment (*1*) measured the background radio noise reaching the radar receiver at a wavelength of 17 cm. Its radar antenna, fixed to the spinning spacecraft, made two such background measurements each 12-second rotation, one while the antenna was pointing down to the hot planet (the planet calibration) and the other while the antenna was pointing outward to cold space (the space calibration). During a typical daily orbital pass, over 300 pairs of such radiometric measurements were made, their primary use being to monitor receiver performance, which proved to be extremely stable. Because of the inclined orbit, coverage was restricted to planetary latitudes between 75°N and 75°S. Nonetheless, because the planet rotated under the orbital plane during the experiment's 28-month lifetime, 94 percent of the planetary surface was observed.

The antenna "footprint," the area of planetary surface filling the beam during a planet calibration measurement, was determined by the antenna's 30° acceptance cone angle, being 90 km in diameter at the lowest periapsis altitude of 150 km and increasing nearly linearly with altitude as the spacecraft climbed to the maximum radar operating limit of 4700 km. This variation is in contrast with that of the radar altimeter's footprint, which was largely controlled by the radar waveform, rising from 7 by 23 km at 200-km altitude near periapsis to about 100-km diameter at 4000-km altitude (*2*).

The global map of the planet calibration data is shown in Fig. 1, where the featureless background has a brightness temperature of about 635 K (*3*). Areas darker than their surroundings denote a reduction in received thermal flux; the gradual darkening below 50°S results from an increasing angular offset of the antenna from nadir during the planet calibration in that region, caused by an antenna steering limitation (*1*), whereas localized dark regions are associated with reduced thermal emission from the surface. These latter areas have brightness temperatures ranging down to 405 K and correspond closely with elevated regions located by the radar altimeter (*2*). The areas of reduced emission are associated with Theia Mons at 282°E, 23°N; Maxwell Mons at 5°E, 63°N; Aphrodite Terra at 95°E, 5°S and at 125°E, 10°S; and Ozza Mons at 200°E, 2°N. The diameter of the footprint at Theia Mons is 95 km, at Maxwell Mons is 1100 km, and varies from 110 to 130 km for the remaining features.

The physical surface temperature of the median plains, which lie within 1 km of the median planetary radius of 6051.6 km and cover some 80 percent of the surface of Venus, has been determined by the Venera landers (*4*) and by the Pioneer Venus probes (*5*) to be 735 ± 10 K. On the basis of the global altitude measurements of the Pioneer Venus radar and the nearly adiabatic lapse rate of −9 K/km determined by the Venera and Pioneer Venus probes, Theia Mons and the equatorial highlands at a radius of about 6056 km should be 40 K colder than the median plains, an effect that would be barely discernible in Fig. 1, where the statistical measurement errors approach 15 K. How, then, can we explain the substantially cooler emission temperatures actually observed?

The thermal power emitted by an object at radio wavelengths, where the Rayleigh-Jeans approximation to the emission law is valid, depends on the product of its physical temperature (T_p) and its emissivity (e). When viewed from above, the total power seen from a planet per unit surface area will be the sum of an emitted and a reflected component and will, in general, vary with θ, the angle of incidence to the local surface normal at which the observation is made.

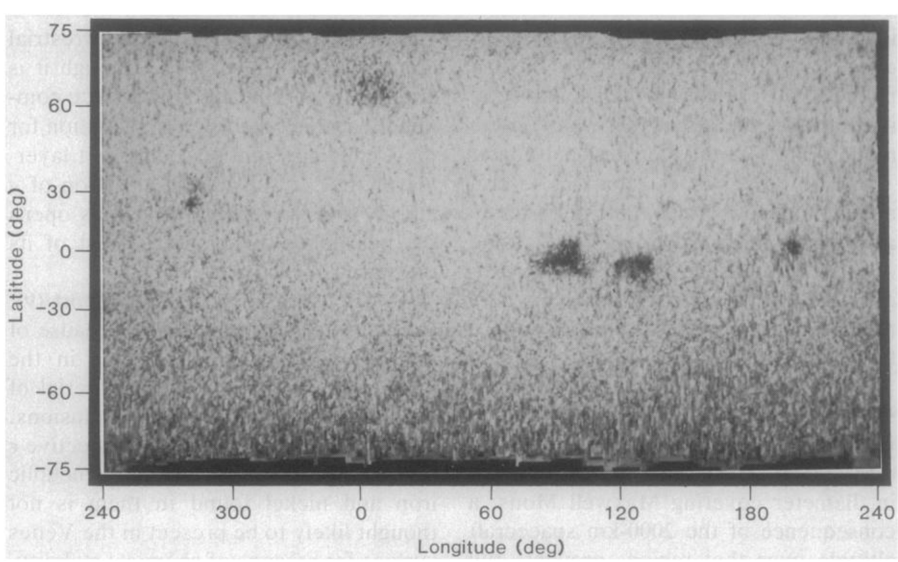

Fig. 1. Radio brightness temperatures of Venus at 17-cm wavelength as observed by the Pioneer Venus radar mapper experiment. The brightness temperature of most of the planet's surface has been taken to be 635 K; under this assumption, the darkest (coolest) areas have a brightness temperature of 405 ± 30 K.

It is convenient to express this total power in terms of an apparent brightness temperature (T_b), defined to be that temperature which would yield the observed power if the observed area were a perfect blackbody thermal emitter (unit emissivity). Considerations of detailed thermodynamic balance and conservation of energy require a relationship between the actual e and reflectivity (ρ') (*6*) such that

$$e(\theta) = 1 - \rho'(\theta) \qquad (1)$$

where $\rho'(\theta)$ represents the fraction of the power incident at angle θ that is reflected or scattered by the surface. It is clear, therefore, that a measurement of e yields a determination of ρ' that can be combined with direct radar measurements to increase our knowledge of surface properties.

In the case of Venus, where the surface is overlain by a thick atmosphere of CO_2, it is convenient to approximate the apparent T_b seen by an observer above the atmosphere (*7*) as

$$T_b = T_p[e + \alpha(1 - e)(2 - \alpha)] \qquad (2)$$

where α is the one-way attenuation suffered by a radio signal passing through the Venus atmosphere at the specified angle of incidence. Both e and α are thus functions of θ. Furthermore, e will, in general, also be a function of the polarization at which the observation is made. Thus, from Eq. 2 it is clear that, if T_p and α are known, a measurement of T_b yields a determination of e.

Gale *et al.* (*8*) have developed an empirical expression for α that is in good agreement with most observations of the Venus atmosphere in the centimeter-decimeter wavelength range. At a wavelength of 17 cm, this expression gives $\alpha = 0.05$ for observations of the median plains at angles near normal incidence; it is clear that the atmosphere has only a modest effect on the Pioneer Venus data.

The low T_b values seen in several areas on Venus thus almost certainly arise from a correspondingly low value of e. This conclusion is further strengthened by the correlation between cool regions of Fig. 1 and regions of high ρ found by Pettengill *et al.* (*9*).

Applying Eq. 2 to the coolest areas shown along the equator in Fig. 1, where $T_b = 405 \pm 30$ K (*3*), yields $e = 0.54 \pm 0.05$. The large footprint 1100 km in diameter covering Maxwell Mons, a consequence of the 2000-km spacecraft altitude over that region, prevents full resolution of the region of low e presumably associated with that feature and, for the same reason, explains the absence of thermal noise signatures for other smaller elevated northern features surrounding Lakshmi Planum such as Akna and Freia Mons (*9*).

It is clear from this discussion that radio emission measurements enhance and complement the radar-altimeter ρ results. The latter are more useful when measuring low values of reflectivity ($\rho < 0.2$), whereas the former are more reliable for high values ($\rho > 0.2$), because of the relation $e = 1 - \rho'$. Furthermore, in addition to a possibly higher intrinsic measurement accuracy, the estimate of e obtained from radiometry is more directly tied to the inherent electrical properties of the near-surface material than the radar-determined ρ. The improvement stems from the difference between ρ and ρ' (*6*) and the difficulty in obtaining the full scattering function for a particular surface region from radar-backscattering observations alone.

When viewed at normal incidence, a smooth surface forming the interface between vacuum and a homogeneous material characterized by unit magnetic permeability and a complex dielectric constant (ϵ) yields an emissivity

$$e = \frac{4\,\mathbf{Re}\,(\epsilon^{1/2})}{|1 + \epsilon^{1/2}|^2} \qquad (3)$$

If ϵ is real, the inferred value $e = 0.54 \pm 0.05$, for the coolest regions of Fig. 1 leads to $\epsilon = 27 \pm 7$ for the corresponding near-surface material. By contrast, $\epsilon = \sim 5$ for the median plains (*10*). Equation 3 assumes that quasi-coherent subsurface layers play no important role in controlling e; Fisher and Staelin (*11*) have shown how such layers, if present, may reduce the effective e of a surface, an effect believed to explain the low e values occasionally seen in terrestrial arctic ice and snow (*12*). Although it is impossible to rule out this effect completely at this time as an explanation for the Venus observations, coherent layering predicts a substantial variation of e and ρ' with wavelength and thus opens the possibility for a specific test of its presence.

As discussed in our earlier report (*9*), we believe that the most likely cause of an ϵ value as high as 27 lies in the presence within the surface material of small electrically conducting inclusions. Many meteorites display high effective ϵ for just this reason, although the metallic iron and nickel found in them is not thought likely to be present in the Venus surface for reasons of chemical stability. At present, the most likely candidate for the conducting material on Venus seems to be iron sulfide, primarily pyrites.

How did this material find its way to the surface of Venus, and why is it distributed preferentially at the higher elevations? If the origin of the elevated regions is primarily volcanic as has been suggested by several investigators (*13*), one might expect substantial quantities of pyrites in association with the upwelling magma. At the surface these would be chemically degraded by small amounts of water vapor in the atmosphere, but aeolian scouring might maintain fresh supplies of pyrite-laden material near enough to the surface to support the high observed ρ.

PETER G. FORD
GORDON H. PETTENGILL
Department of Earth and Planetary Sciences, Massachusetts Institute of Technology, Cambridge 02139

References and Notes

1. G. H. Pettengill, D. F. Horwood, C. H. Keller, *IEEE Trans. Geosci. Remote Sensing* **GE-18**, 28 (1980).
2. G. H. Pettengill, E. Eliason, P. G. Ford, G. B. Loriot, H. Masursky, G. E. McGill, *J. Geophys. Res.* **85**, 8261 (1980).
3. On the basis of ground-based radiometric observations, G. L. Berge, D. O. Muhleman, and G. S. Orton [*Icarus* **17**, 678 (1972)] have determined that the disk T_b of Venus at a wavelength of 21 cm is 617 ± 25 K. In the calibration of the spacecraft radiometric observations, we have assumed that the median plains have a reflectivity $\rho'(0) = 0.15 \pm 0.03$ (*9, 10*) and a T_p of 735 ± 10 K (*4, 5*), which leads through Eq. 2 to a predicted T_b of 635 K for these regions. Supporting this calibration are solar radiation measurements obtained by the radar experiment every 224 days as the sun moved into the direction of the space calibrations made near the ecliptic. Although the latter do not in themselves provide a highly accurate calibration of the radiometric system, they are consistent to within 10 percent with the basic calibration and are independent of planetary assumptions. The zero level of the calibration was obtained from the space-calibration observations. The statistical error associated with the spacecraft observations of temperature at the near-equatorial surface resolution of about 200 km presented in Fig. 1 is about 15 K. The errors quoted in our results have been enlarged to include the estimated errors of calibration.
4. M. Ya. Marov, *Annu. Rev. Astron. Astrophys.* **16**, 147 (1978).
5. A. Seiff, D. B. Kirk, R. E. Young, R. C. Blanchard, J. T. Findlay, G. M. Kelley, S. C. Sommer, *J. Geophys. Res.* **85**, 7903 (1980).
6. The detailed balance theorem of thermodynamics requires that $e(\theta) = a(\theta)$, where a is the absorptivity and θ is the angle at which the emitted energy is observed or the irradiating energy impinges. Let us now define an integrated surface reflectivity given by

$$\rho'(\theta) = (\sec\theta/4\pi) \int_{2\pi} \sigma(\theta,\theta',\phi')\,d\Omega'$$

where $\sigma(\theta,\theta',\phi')/4\pi$ is the area-normalized radar scattering cross section for energy in a given polarization state arriving from direction θ and scattered into a direction defined by polar angles θ' and ϕ' per unit solid angle Ω', and the integral is taken over the hemisphere $0 \leq \theta' \leq \pi/2$. From conservation of energy it is clear that $\alpha(\theta) = 1 - \rho'(\theta) = e(\theta)$. The radar-derived reflectivity (ρ) is also obtained by integrating σ over a range of scattering angles [see, for example, T. Hagfors, *Radio Sci.* **5**, 189 (1970)], but the range of these angles usually accessible to radar measurement is limited by the available observing geometry. If the surface undulates smoothly in a manner that retains coherence in the scattered energy, the theory used to extract reflectivity from the radar data is generally capable of yielding ρ values that are comparable to the total reflectivity ρ'. But ρ will be smaller than the true ρ', to the extent that the surface contains small structure capable of producing incoherent diffuse scattering spread widely over the hemisphere of sky.

7. A general expression for T_b, the apparent brightness temperature seen looking down at the planet from outside the atmosphere at radio wavelengths, may be written as

$$T_b = (1 - \alpha)\{eT_p + \rho'[\alpha T_a + (1 - \alpha)T_s]\} + \alpha T_a$$

where e is the surface emissivity, ρ' is the surface reflectivity (6), T_a is the effective physical temperature of the atmosphere, and T_s is the sky brightness temperature. The quantities α, e, and ρ' will depend on the angle at which the surface is being observed. This expression approximates the temperature-weighted integration of σ over the sky, as seen from the surface, by the simple product of ρ' and T_s in the direction corresponding to specular reflection. For Venus, this approximation should be adequate. The expression above may be further simplified by noting that, at wavelengths of interest here, the atmospheric interaction takes place almost entirely in the bottom scale height, where $T_a \simeq T_p$. Furthermore, T_s is only about 4 K at decimetric wavelengths (barring an accidental alignment with the sun) and can be neglected to our level of accuracy. Combining these terms and using $\rho' = 1 - e$, we obtain Eq. 2.

8. W. Gale, M. Liwshitz, and A. C. E. Sinclair [*Science* **164**, 1059 (1969)] quote an empirical expression (modified slightly to better fit modern data)

$$\alpha = 1 - \exp(-15/\lambda^2)$$

where λ is the wavelength in centimeters, that specifies the one-way attenuation suffered by radio waves in penetrating the Venus atmosphere at normal incidence to the Venus surface lying at mean altitude.

9. G. H. Pettengill, P. G. Ford, S. Nozette, *Science* **217**, 640 (1982).
10. G. H. Pettengill, *Annu. Rev. Astron. Astrophys.* **16**, 265 (1978).
11. A. D. Fisher and D. H. Staelin, *Icarus* **32**, 98 (1977).
12. K. F. Kunzi, A. D. Fisher, D. H. Staelin, J. W. Waters, *J. Geophys. Res.* **81**, 4965 (1976).
13. R. S. Saunders and M. C. Malin, *Geophys. Res. Lett.* **4**, 547 (1977); H. Masursky, E. Eliason, P. G. Ford, G. E. McGill, G. H. Pettengill, G. G. Schaber, G. Schubert, *J. Geophys. Res.* **85**, 8232 (1980).
14. We thank D. H. Staelin for stimulating discussions on the relationship between surface properties and emissivity. This research was supported by a contract with the NASA Ames Research Center.

20 December 1982; revised 8 February 1983

Stable Nitrogen Isotope Ratios of Bone Collagen Reflect Marine and Terrestrial Components of Prehistoric Human Diet

Abstract. *The $\delta^{15}N$ values of bone collagen from Eskimos and from Northwest Coast Indians dependent on salmon fishing are about 10 per mil more positive than those from agriculturalists in historic times. Among prehistoric humans, two groups dependent on marine food sources show bone collagen $\delta^{15}N$ values that are 4 to 6 per mil more positive than those from two agricultural groups. The nitrogen isotope ratios of bone collagen from prehistoric inhabitants of the Bahamas are anomalously low for reasons that relate to the biogeochemical cycle of nitrogen in coral reefs.*

Knowledge of diet yields information about human social and economic organization, health, and way of life (*1*). Generally, prehistoric human diets have been reconstructed from determinations of the abundance of floral and faunal remains in archeological deposits (*2*). Recently, analyses of trace elements and stable isotopes in human bone have been applied to the problem (*3–7*). We have shown that there is a large difference in the $^{15}N/^{14}N$ ratios of bone collagen between animals feeding in marine systems and those feeding solely on terrestrial foods (Table 1) (*8*). We now report that stable nitrogen isotope ratios of bone collagen can be used in reconstructing the relative amounts of marine and terrestrial food sources in diets of historic and prehistoric human populations.

A study (*7*) of animals raised on diets for which the nitrogen isotopic compositions were known showed that the $^{15}N/^{14}N$ ratios of animal tissues are determined by the $^{15}N/^{14}N$ ratios of their diets. Diet nitrogen isotope ratios ultimately depend on the $^{15}N/^{14}N$ ratios of plants at the base of the food chain. Marine plants have higher $^{15}N/^{14}N$ ratios than terrestrial plants (*9, 10*), and this difference in ^{15}N content is carried up food chains, causing marine animals to have higher $^{15}N/^{14}N$ ratios than those of terrestrial animals (*8, 10, 11*). The $^{15}N/^{14}N$ ratios of bone collagen of humans feeding on marine food sources should thus be higher than those of peoples subsisting on terrestrial food sources.

We determined isotopic compositions of bone collagen of several individuals from each of four groups of historic human populations (*12*) known to have exploited primarily either marine or terrestrial food sources. These included (i) Alaskan Eskimos, whose diet was composed of nearly 85 percent marine mammals (*13*); (ii) Haida and Tlingit Indians from the Northwest Coast of the United States, who depended more on salmon fishing for food than on all other subsistence techniques combined (*14*); (iii) Havihuh agriculturalists from New Mexico; and (iv) manioc farmers from Colombia, South America. Agricultural products provided almost the entire diet for the latter two groups (*14*).

Prehistoric groups from North America, South America, and Europe were also studied. The inhabitants of the Mugu site just north of Los Angeles, California, lived on the coast all year and subsisted largely on marine fish and mammals with plants from the surrounding countryside as supplements (*15*). The Danish Mesolithic period people also lived on the coast and apparently used large quantities of marine foods, as suggested by archeological evidence and the stable carbon isotope ratios of bone collagen (*6*). The Neolithic period people from Europe depended largely on grains that they grew (*6*), while the agriculturalists from the site of Tehuacán in Mexico depended primarily on maize (*2*). The Bahamian peoples, from sites on several islands in the central Bahamas, exploited molluscs and fish in the reef system and also used some agricultural products, although there is disagreement whether these were primarily maize or manioc (*16*).

Table 1. The $\delta^{15}N$ and $\delta^{13}C$ values (*8, 19*) of bone collagen from animals feeding exclusively on marine or terrestrial food sources. Two marine birds could not be classified as either fish or mollusc eaters. Abbreviation: S.D., standard deviation.

Animal	Sample (*N*)	$\delta^{15}N$ (per mil)			$\delta^{13}C$ (per mil)		
		Mean	S.D.	Range	Mean	S.D.	Range
				Terrestrial			
Mammals and birds	25	+5.9	2.3	+1.9, +10.0	−18.6	3.1	−22.5, −11.9
Herbivores	19	+4.9	1.6	+1.9, +7.3	−19.3	3.1	−22.5, −11.9
Carnivores	6	+8.0	1.6	+5.9, +10.0	−18.4	2.1	−21.2, −15.8
				Marine			
Mammals	41	+15.6	2.2	+11.7, +22.9	−13.1	1.6	−16.1, −9.6
Fish eaters	25	+16.7	1.8	+14.3, +22.9	−12.8	1.1	−15.2, −11.0
Plankton, mollusc, arthropod eaters	16	+13.8	1.5	+11.7, +16.6	−13.5	2.2	−16.1, −9.6
Birds	11	+13.0	2.8	+9.4, +17.9	−16.2	2.5	−19.6, −12.1
Fish eaters	4	+16.2	1.6	+14.2, +17.9	−15.2	2.3	−18.6, −13.6
Mollusc eaters	5	+10.9	1.3	+9.4, +13.0	−17.1	1.8	−19.0, −14.9
Fish	10	+13.8	1.6	+11.1, +16.0	−12.5	1.4	−14.4, −10.0